Fingerprints of the COVID-19 economic downturn and recovery on ozone anomalies at high-elevation sites in North America and western Europe

Davide Putero, Paolo Cristofanelli, Kai-Lan Chang, Gaëlle Dufour, Gregory Beachley, Cédric Couret, Peter Effertz, Daniel Jaffe, Dagmar Kubistin, Jason Lynch, et al.

Atmos. Chem. Phys., 23, 15693–15709, 2023
https://doi.org/10.5194/acp-23-15693-2023

Atmospheric Chemistry and Physics
Open Access
EGU

Fingerprints of the COVID-19 economic downturn and recovery on ozone anomalies at high-elevation sites in North America and western Europe

Davide Putero[1], Paolo Cristofanelli[2], Kai-Lan Chang[3], Gaëlle Dufour[4], Gregory Beachley[5], Cédric Couret[6], Peter Effertz[7], Daniel A. Jaffe[8], Dagmar Kubistin[9], Jason Lynch[5], Irina Petropavlovskikh[7], Melissa Puchalski[5], Timothy Sharac[5], Barkley C. Sive[10], Martin Steinbacher[11], Carlos Torres[12], and Owen R. Cooper[3]

[1]National Research Council of Italy – Institute of Atmospheric Sciences and Climate, CNR–ISAC, Turin, Italy
[2]National Research Council of Italy – Institute of Atmospheric Sciences and Climate, CNR–ISAC, Bologna, Italy
[3]Cooperative Institute for Research in Environmental Sciences, University of Colorado Boulder/NOAA Chemical Sciences Laboratory, Boulder, USA
[4]Université de Paris Cité and Univ. Paris Est Créteil, CNRS, LISA, Paris, France
[5]Office of Atmospheric Protection, U.S. Environmental Protection Agency, Washington DC, USA
[6]German Environment Agency, Zugspitze, Germany
[7]Cooperative Institute for Research in Environmental Sciences, University of Colorado Boulder/NOAA Global Monitoring Laboratory, Boulder, USA
[8]University of Washington, School of STEM/Department of Atmospheric Sciences, Bothell/Seattle, USA
[9]Hohenpeißenberg Meteorological Observatory, Deutscher Wetterdienst, Hohenpeißenberg, Germany
[10]Air Resources Division, National Park Service, Denver, USA
[11]Empa, Laboratory for Air Pollution & Environmental Technology, Dübendorf, Switzerland
[12]Izaña Atmospheric Research Center, State Meteorological Agency of Spain, IARC-AEMET, Tenerife, Spain

Correspondence: Davide Putero (d.putero@isac.cnr.it)

Received: 2 August 2023 – Discussion started: 16 August 2023
Revised: 25 October 2023 – Accepted: 13 November 2023 – Published: 21 December 2023

Abstract. With a few exceptions, most studies on tropospheric ozone (O_3) variability during and following the COrona VIrus Disease (COVID-19) economic downturn focused on high-emission regions or urban environments. In this work, we investigated the impact of the societal restriction measures during the COVID-19 pandemic on surface O_3 at several high-elevation sites across North America and western Europe. Monthly O_3 anomalies were calculated for 2020 and 2021, with respect to the baseline period 2000–2019, to explore the impact of the economic downturn initiated in 2020 and its recovery in 2021. In total, 41 high-elevation sites were analyzed: 5 rural or mountaintop stations in western Europe, 19 rural sites in the western US, 4 sites in the western US downwind of highly polluted source regions, and 4 rural sites in the eastern US, plus 9 mountaintop or high-elevation sites outside Europe and the United States to provide a "global" reference. In 2020, the European high-elevation sites showed persistent negative surface O_3 anomalies during spring (March–May, i.e., MAM) and summer (June–August, i.e., JJA), except for April. The pattern was similar in 2021, except for June. The rural sites in the western US showed similar behavior, with negative anomalies in MAM and JJA 2020 (except for August) and MAM 2021. The JJA 2021 seasonal mean was influenced by strong positive anomalies in July due to large and widespread wildfires across the western US. The polluted sites in the western US showed negative O_3 anomalies during MAM 2020 and a slight recovery in 2021, resulting in a positive mean anomaly for MAM 2021 and a pronounced month-to-month variability in JJA 2021 anomalies. The eastern US sites were also characterized by below-mean O_3 for both MAM and JJA 2020, while in 2021 the negative values exhibited

an opposite structure compared to the western US sites, which were influenced by wildfires. Concerning the rest of the world, a global picture could not be drawn, as the sites, spanning a range of different environments, did not show consistent anomalies, with a few sites not experiencing any notable variation. Moreover, we also compared our surface anomalies to the variability of mid-tropospheric O_3 detected by the IASI (Infrared Atmospheric Sounding Interferometer) satellite instrument. Negative anomalies were observed by IASI, consistent with published satellite and modeling studies, suggesting that the anomalies can be largely attributed to the reduction of O_3 precursor emissions in 2020.

1 Introduction

Tropospheric ozone (hereafter simply referred to as O_3) is a short-lived climate forcer (Szopa et al., 2021) that plays a key role in the climate system. It is one of the most powerful anthropogenic greenhouse gases (the third most important, after carbon dioxide and methane), and it also impacts the lifetime of methane, which is one of the O_3 precursors (Monks et al., 2015; Gulev et al., 2021). Moreover, at the surface it also has adverse effects on ecosystems, crop productivity, and human health (Fleming et al., 2018; Mills et al., 2018).

The COrona VIrus Disease (COVID-19) pandemic emerged in late 2019 and initiated a global economic downturn in 2020, which was characterized by a drastic reduction of emissions related to several sectors, such as private transportation and both domestic and international aviation (e.g., Le Quéré et al., 2020; Friedlingstein et al., 2022). The reduction of emissions turned into a reduction of air pollutants that can directly be related to O_3 variability due to its photochemical formation from O_3 precursors, such as nitrogen oxides (NO and NO_2), carbon monoxide (CO), and non-methane volatile organic compounds (NM-VOCs).

Several studies in the past few years have investigated the impact of the COVID-19 economic downturn on O_3 concentrations and variability at global, regional, and local scales (Gkatzelis et al., 2021; Sokhi et al., 2021). However, most of these works focused on high-emission sources or urban environments (Sicard et al., 2020; Adam et al., 2021; Chossière et al., 2021; Keller et al., 2021). A number of studies indicated varying O_3 behavior as a function of the reduction in the emissions, mainly dependent on whether the photochemical O_3 formation in the considered regions was NO_x- or VOC-limited (Gaubert et al., 2021; Matthias et al., 2021; Mertens et al., 2021; Cuesta et al., 2022).

Concerning free-tropospheric values, which could be considered representative of background atmospheric conditions, Steinbrecht et al. (2021) reported a reduction of O_3 of 7 % ($\sim$ 4 ppb) from April to August 2020 in the 1–8 km altitude region of northern midlatitudes with respect to the 2000–2020 climatological mean. Cristofanelli et al. (2021) observed reductions in the 2020 monthly mean O_3 values (with respect to a 25-year climatological mean) at a mountaintop site in Italy. Other studies have indicated the presence of negative O_3 anomalies in the free troposphere in 2020, mainly as a consequence of emissions reductions (Bouarar et al., 2021; Clark et al., 2021; Miyazaki et al., 2021). Chang et al. (2022) determined that the free-tropospheric O_3 negative anomalies in 2020 were the most profound since 1994 for both Europe and western North America and that the 2020 anomalies had a weakening influence on the 1994–2019 positive O_3 trends above these regions. The O_3 reductions in the free troposphere were also confirmed by the work of Ziemke et al. (2022), in which satellite measurements of tropospheric column O_3 show that the 2020 negative anomalies in the Northern Hemisphere occurred again in spring–summer 2021.

In this study, we analyzed the O_3 variability at 41 high-elevation sites across the globe, representative of different environments and emission source regions, during the COVID-19 economic downturn. The aim of this work is to determine if the negative O_3 anomalies observed in the free troposphere (e.g., Bouarar et al., 2021; Clark et al., 2021; Steinbrecht et al., 2021; Chang et al., 2022; Ziemke et al., 2022) also occurred in the boundary layer by focusing on a selection of mountaintop and high-elevation monitoring sites with available data up to December 2021. Therefore, our study will cover both the COVID-19 economic downturn in 2020 and the following year of 2021, which was associated with a recovery of emissions representative of a pre-pandemic level.

The paper is structured as follows. Section 2 will present the methodologies adopted, Sect. 3 will focus on the discussion of the results obtained, and conclusions will be drawn in Sect. 4.

2 Methods

2.1 Surface ozone

Figure 1 shows the geographical location of the sites considered in this study, and additional details (station name, latitude, longitude, and elevation) for each station are reported in Table 1. Hereafter we will refer to each site by using its acronym (code), also listed in Table 1. The stations comprise a selection of 41 high-elevation sites worldwide, representative of five different environments (the so-called "regions" in Table 1 and Fig. 1), i.e., (i) 5 European rural or mountaintop sites (EUR), (ii) 19 sites in the western US representative

of rural conditions (WUS_R), (iii) 4 sites in the western US downwind of highly polluted source areas (WUS_P), (iv) 4 eastern US rural sites (EUS), and (v) 9 other globally distributed mountaintop or high-elevation sites (OT). The OT sites are representative of very different environments (e.g., Antarctic conditions compared to the tropical latitudes of Mt. Kenya or Mauna Loa); however, these sites provide a characterization of baseline O_3 variability in several regions of the world that are far away from major anthropogenic emissions.

At all of the considered sites the UV-absorption method is used for measuring surface O_3, and common guidelines are followed for the reliability and consistency of O_3 data among the different monitoring programs (e.g., Galbally et al., 2013). With the exception of MBO, the 27 high-elevation monitoring sites in the US are Clean Air Status and Trends Network (CASTNET) sites maintained by the Environmental Protection Agency (EPA) and the National Park Service (NPS). The remaining 14 sites are all part of the Global Atmosphere Watch program of the World Meteorological Organization (WMO/GAW), including 9 global stations, 4 regional stations, and 1 contributing station. The data processing involved, when necessary, re-formatting the data, time shifting to UTC (all measurements hereby presented refer to UTC), and unit conversions. Similar to the methods of Cooper et al. (2020) and Cristofanelli et al. (2020), the ZSF time series shown here is derived from merging the observations carried out at both Zugspitze summit and the Schneefernerhaus station (see more details in the Supplement).

2.1.1 Surface ozone data selection

As our study focuses on the quantification of O_3 anomalies at high-elevation and remote locations, careful data selection was carried out to focus on well-mixed atmospheric conditions and to also avoid times of the day that can be influenced by fresh anthropogenic emissions that can lead to the localized production or destruction of O_3 (Cooper et al., 2020). As the sites in Fig. 1 are representative of very different environments, the analysis of the diurnal cycles led to the identification of the following conditions for data selection.

- Nighttime (i.e., between 20:00 and 07:59 local time) data for mountaintop and stations above 1500 m a.s.l. This selection was chosen to focus on regionally representative O_3, and to avoid the presence of local air masses that are transported, during daytime, from the valleys up to the mountaintops by upslope winds (Price and Pales, 1963; Cooper et al., 2020; Cristofanelli et al., 2020). This condition was valid for all of the European sites above 1500 m a.s.l., for some of the OT sites (MLO, TLL, IZO, MKN and PDI), and MBO.

- Maximum daily 8 h average (MDA8) O_3 values for all of the US EPA and NPS sites (i.e., all stations belonging to WUS_R, WUS_P, and EUS, except MBO). This was chosen as these stations can experience surface deposition at nighttime, which can therefore lower the O_3 values. MDA8 values are typically characteristic of the time of the day when the boundary layer is well mixed and are therefore representative of a broad region around each measurement site.

- Daily mean data for HPB, SUM, and the two stations in Antarctica (DCC and SPO); the latter three sites are characterized by almost no diurnal O_3 cycle, and therefore all data from the full 24 h record can be used.

2.1.2 Trend detection and calculation of the anomalies

To describe and quantify the effects of the COVID-19 economic downturn on O_3 values, we computed monthly O_3 anomalies at each of the selected sites, derived after removing the seasonal and trend components from the O_3 monthly means. The deseasonalization allows the production of a more precise trend with less uncertainty and avoids estimation bias due to missing data. Similar to Cooper et al. (2020) and Cristofanelli et al. (2020), we followed several steps to calculate the monthly O_3 anomalies (also summarized in Fig. S1 in the Supplement).

First, we determined the monthly O_3 means for each site, setting a threshold of 50 % on hourly data availability for each month. We also carried out a sensitivity study by adopting a different threshold (i.e., 66 %) or by extending the threshold to daily means before calculating monthly values. The sensitivity study produced no significant variation in our results (see Fig. S2 in the Supplement). The choice of a more relaxed 50 % threshold was made for retaining enough data at several sites, such as MKN, MBO, or PDI, which could encounter various issues that prevented the collection of complete data samples each month.

Second, we computed the "climatological year", composed of the 20-year mean for each of the 12 months. The baseline period for the 20-year mean is 2000–2019; shorter periods were used if data availability was limited (see Table 1 for the different starting years).

Then, we obtained the "monthly differences", i.e., the month-by-month differences between the monthly means and the corresponding months of the climatological year.

Last, we used the monthly differences for quantifying the long-term O_3 changes and also to compute the monthly anomalies (i.e., deseasonalized and detrended monthly means) in order to further compare the consistency of the COVID-19 impact at different sites. We used quantile regression for evaluating the trends (and choosing the 50th percentile, i.e., equivalent to the median regression), which is recommended as a standard approach for trend analysis for the TOAR-II activity (Chang et al., 2023b). It is a well-suited technique for detecting heterogeneous distributional changes (Chang et al., 2021) and can incorporate covariates such as piecewise trends for change point analysis. Although

Table 1. List of the stations used in this study for calculating the monthly anomalies, also reported in Fig. 1. Trend values (50th percentile, in ppb per decade) are calculated by using quantile regression and reported together with 95 % confidence intervals and p values, computed by adopting the moving block bootstrap algorithm (see Sect. 2.1.2). Period indicates the range of years considered for the trend calculation. The region abbreviations are as follows: WUS_R – western US "rural", WUS_P– western US "polluted", EUS – eastern US, EUR – Europe, OT – other.

Site name	Code	Lat. (°N)	Long. (°E)	Elevation (m a.s.l.)	Region	Period	Trend (ppb per decade)
Glacier National Park	GNP	48.51	−114.00	976	WUS_R	2000–2021	1.30 [±1.10], $p = 0.02$
Yellowstone National Park	YEL	44.56	−110.40	2400	WUS_R	2000–2021	−1.54 [±0.90], $p < 0.01$
Mount Bachelor Observatory	MBO	43.98	−121.69	2763	WUS_R	2004–2021	2.82 [±2.23], $p = 0.01$
Grand Teton National Park	GTP	43.67	−110.60	2105	WUS_R	2011–2021	−1.28 [±2.74], $p = 0.35$
Wind Cave National Park	WNC	43.56	−103.48	1288	WUS_R	2005–2021	−0.67 [±1.54], $p = 0.39$
Craters of the Moon National Monument	CRA	43.47	−113.56	1815	WUS_R	2000–2021	−1.21 [±1.34], $p = 0.03$
Pinedale	PND	42.93	−109.79	2388	WUS_R	2000–2021	−1.38 [±0.74], $p < 0.01$
Centennial	CNR	41.36	−106.24	3178	WUS_R	2000–2021	−1.65 [±1.05], $p < 0.01$
Lassen Volcanic National Park	LAV	40.54	−121.58	1756	WUS_R	2000–2021	−1.28 [±0.82], $p < 0.01$
Dinosaur National Monument	DIN	40.44	−109.30	1463	WUS_R	2007–2021	−0.27 [±2.20], $p = 0.81$
Rangely	RAN	40.09	−108.76	1655	WUS_R	2010–2021	−2.30 [±2.49], $p = 0.07$
Great Basin National Park	GBN	39.00	−114.22	2058	WUS_R	2000–2021	−0.26 [±0.80], $p = 0.51$
Gothic	GTH	38.96	−106.99	2926	WUS_R	2000–2021	−1.56 [±0.91], $p < 0.01$
Canyonlands National Park	CAN	38.46	−109.82	1794	WUS_R	2000–2021	−1.87 [±0.98], $p < 0.01$
Mesa Verde National Park	MEV	37.20	−108.49	2170	WUS_R	2000–2021	−0.22 [±1.01], $p = 0.66$
Zion National Park	ZIO	37.20	−113.15	1213	WUS_R	2004–2021	−2.11 [±0.97], $p < 0.01$
Grand Canyon National Park	GRC	36.06	−112.18	2073	WUS_R	2000–2021	−2.06 [±0.90], $p < 0.01$
Petrified Forest National Park	PFN	34.82	−109.89	1712	WUS_R	2002–2021	−1.86 [±0.91], $p < 0.01$
Chiricahua National Monument	CNM	32.01	−109.39	1570	WUS_R	2000–2021	−1.13 [±1.13], $p = 0.05$
Rocky Mountain National Park	RMN	40.28	−105.54	2743	WUS_P	2000–2021	0.12 [±0.81], $p = 0.77$
Yosemite National Park	YOS	37.71	−119.71	1599	WUS_P	2000–2021	−2.65 [±1.68], $p < 0.01$
Sequoia/Kings Canyon National Parks	SQA	36.57	−118.78	1890	WUS_P	2000–2021	−2.51 [±1.84], $p = 0.01$
Joshua Tree National Park	JOT	34.07	−116.39	1244	WUS_P	2000–2021	−1.87 [±1.57], $p = 0.02$
Whiteface Mountain	WFM	44.37	−73.90	1483	EUS	2000–2021	−2.00 [±1.47], $p = 0.01$
Shenandoah National Park	SHN	38.52	−78.44	1073	EUS	2000–2021	−2.84 [±2.03], $p = 0.01$
Cranberry	PNF	36.11	−82.05	1219	EUS	2000–2021	−3.16 [±1.37], $p < 0.01$
Great Smoky Mountains National Park	GSM	35.66	−83.61	1243	EUS	2000–2021	−4.51 [±1.49], $p < 0.01$
Hohenpeißenberg	HPB	47.80	11.01	985	EUR	2000–2021	−1.41 [±1.00], $p = 0.01$
Zugspitze	ZSF	47.42	10.98	2671	EUR	2000–2021	−0.61 [±0.68], $p = 0.13$
Sonnblick	SNB	47.05	12.96	3106	EUR	2000–2021	−1.41 [±0.66], $p < 0.01$
Jungfraujoch	JFJ	46.55	7.99	3580	EUR	2000–2021	−0.70 [±1.04], $p = 0.18$
Monte Cimone	CMN	44.19	10.70	2165	EUR	2000–2021	−2.47 [±1.48], $p < 0.01$
Summit	SUM	72.58	−38.48	3238	OT	2000–2021	−2.37 [±1.19], $p < 0.01$
Denali National Park	DEN	63.72	−148.97	663	OT	2000–2021	0.19 [±0.82], $p = 0.65$
Izaña	IZO	28.31	−16.50	2373	OT	2000–2021	0.17 [±0.84], $p = 0.68$
Pha Din	PDI	21.57	103.52	1466	OT	2014–2021	−4.79 [±11.75], $p = 0.42$
Mauna Loa	MLO	19.54	−155.58	3397	OT	2000–2021	0.35 [±1.45], $p = 0.63$
Mt. Kenya	MKN	−0.06	37.30	3678	OT	2002–2021	1.70 [±2.45], $p = 0.17$
El Tololo	TLL	−30.17	−70.80	2154	OT	2000–2021	2.26 [±0.58], $p < 0.01$
Concordia	DCC	−75.10	123.33	3233	OT	2008–2021	0.32 [±1.05], $p = 0.55$
South Pole	SPO	−90.00	−24.80	2841	OT	2000–2021	1.32 [±0.41], $p < 0.01$

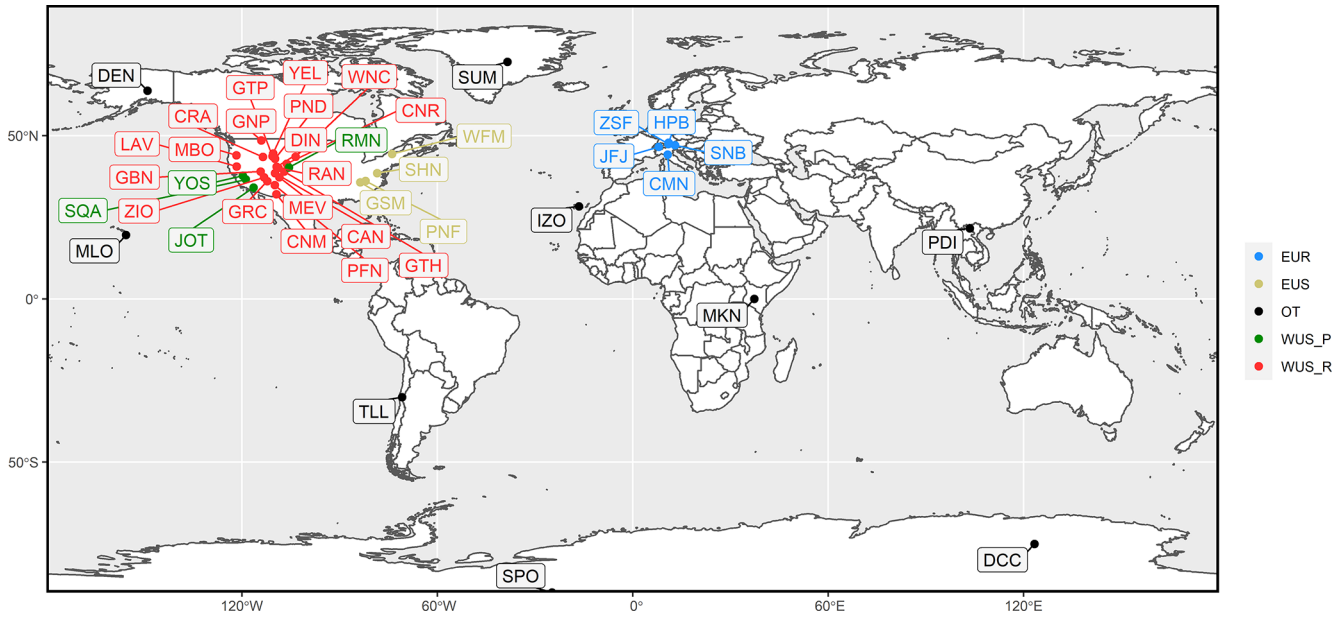

Figure 1. Geographical locations of the sites used in this study (details are reported in Table 1). The region abbreviations are as follows: WUS_R – western US "rural", WUS_P – western US "polluted", EUS – eastern US, EUR – Europe, OT – other.

this study focuses on the impact of the COVID-19 economic downturn in 2020 and 2021, additional years of data will be required to determine if this event is a change point in the long-term trends. To account for autocorrelation and heteroscedasticity, the moving block bootstrap resampling algorithm is implemented (Lahiri, 2003): for each iteration the quantile regression model is fitted to a series of randomly selected block samples and the sampled trend value is extracted. The final trend value (and its uncertainty) was then determined by the mean (and standard deviation) of the sampled trend values. All trends are reported with their 95 % confidence interval and p value.

We also carried out additional analysis to demonstrate the sensitivity of trend estimates based on climatological means or medians. The results are shown in Fig. S3 of the Supplement: although some differences can be seen at individual sites, the general features and conclusions remain the same, indicating that no systematic discrepancies are found between different approaches to estimate the seasonality.

2.2 IASI data

The IASI (Infrared Atmospheric Sounding Interferometer) instrument is a nadir-viewing Fourier transform spectrometer flying on board the EUMETSAT (European Organisation for the Exploitation of Meteorological Satellites) Metop satellites (Clerbaux et al., 2009). The IASI instrument operates in the thermal infrared between 645 and 2760 cm^{-1} with an apodized resolution of 0.5 cm^{-1}. The field of view of the instrument is composed of a 2×2 matrix of pixels with a diameter at nadir of 12 km each. IASI scans the atmosphere with a swath width of 2200 km and crosses the Equator at two fixed local solar times: 09:30 (descending mode) and 21:30 (ascending mode), allowing the monitoring of atmospheric composition twice a day at any location. Three versions of the instrument were built and launched at different times: one aboard the Metop-A platform (October 2006), one aboard the Metop-B platform (September 2012), and one aboard the Metop-C platform (November 2018). Note that Metop-A was deorbited in October 2021.

Ozone profiles used to calculate O_3 partial columns for this study are described in Dufour et al. (2021). A data screening procedure is applied to filter cloudy scenes and to ensure the data quality (Eremenko et al., 2008; Dufour et al., 2010, 2012). It is worth noting that the maximum sensitivity of the retrieved profile in the lower troposphere is around 4 to 6 km (Dufour et al., 2010, 2012). Therefore, we use the lower free-tropospheric column product from 3 to 6 km. Only the morning overpasses of IASI are considered in order to ensure better sensitivity to the lower troposphere. To cover the longest possible period with consistent data, we consider only IASI on Metop-A in this study. A consistency analysis of the IASI-A, IASI-B, and IASI-C time series is needed to use the three instruments simultaneously. Consistent with the surface O_3 measurements, we calculated anomalies for the O_3 partial columns, after removing the seasonality and the trend (see Sect. 2.1.2).

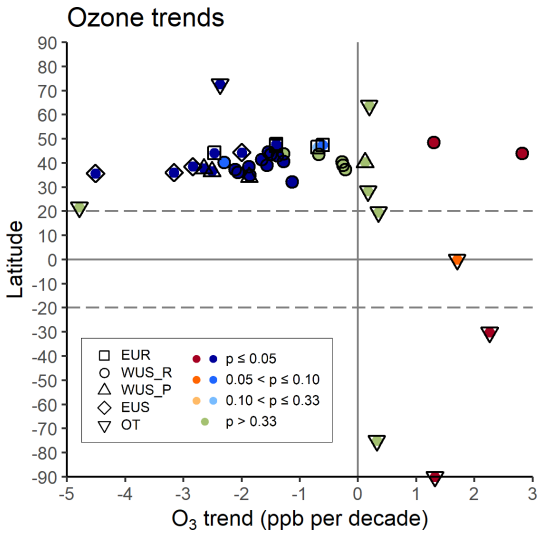

Figure 2. Decadal O_3 trends (50th percentile) for the 41 high-elevation sites used in this study. The reference periods for trend calculation for the different sites are listed in Table 1. Trends are ordered by latitude (y axis), and the colors indicate the sign and p value on the trend, with blue shades for negative trends ($p \leq 0.33$), red shades for positive trends ($p \leq 0.33$), and green for trends of either sign ($p > 0.33$). The shapes identify the different regions, i.e., EUR – Europe, WUS_R – western US "rural", WUS_P – western US "polluted", EUS – eastern US, OT – other.

3 Results and discussion

3.1 Ozone trends

A trend analysis spanning the first 2 decades of the 21st century for long-term observational datasets collected at high-elevation remote and rural locations was performed for most of the stations. The overall picture is reported in Fig. 2, where decadal O_3 trends are reported by latitude and grouped by each of the regions considered in this study (Fig. 1). The calculation period of the trends is 2000–2021 (or shorter for some stations, when data back to 2000 were not available); a recent study (Chang et al., 2023a) has shown that, for MBO, the long-term positive trend was clearly weakened when including the anomalous year 2020 compared to 2004–2019, but the trend rebounded in 2021, between the 5th and 95th percentiles. The variations of the long-term trends at all of the sites, computed by varying the calculation periods of the trends (i.e., 2000–2019, 2000–2020, and 2000–2021), are reported in Table S1. In several cases, the trends did not reveal any relevant impact of the 2020 anomalies, while for 10 sites the 2000–2020 trend was weakened compared to 2000–2019, and a rebound was observed when including 2021. It is interesting to note that for the European sites above 1500 m a.s.l. (i.e., CMN, JFJ, SNB, and ZSF) the long-term trend was weakened when including 2020 and continued to weaken with the addition of 2021 data (see Table S1).

Considering the full 2000–2021 record, the observed trends for the 41 high-elevation sites vary greatly from −4.79 to 2.82 ppb per decade. Decreases in surface O_3 were observed for 30 European and North American sites, with the exceptions of MBO (2.82 ppb per decade) and GNP (1.30 ppb per decade). The trend values for the sites belonging to the OT category showed large differences, with O_3 increases recorded for TLL (2.26 ppb per decade) and MKN (1.70 ppb per decade); on the other hand, PDI (although limited by the rather short reference period) and SUM station showed O_3 decreases (−4.79 and −2.37 ppb per decade, respectively). Both Antarctic sites showed positive trends (SPO: 1.33 ppb per decade, and DCC: 0.32 ppb per decade), which are in line with previous studies described in Kumar et al. (2021). It has to be noted that the trend at DCC could be affected by the large data gap in the measurements between 2014 and 2016, and this will certainly need further investigation.

The trends for most of the sites in western North America considered in this study were previously reported by Chang et al. (2023a), although considering a slightly longer period (1995–2021). Their results are consistent with the ones reported in Fig. 2 for the WUS_R and WUS_P categories, indicating that the majority of the sites in western North America show a consistent pattern of negative trends, pointing to an overall decrease in regional boundary layer O_3. The clear outlier is MBO, but this site is uniquely situated on the summit of an isolated mountain. During nighttime conditions reported here, MBO is strongly influenced by the lower free troposphere, which has experienced a small increase in O_3 since the 1990s (Chang et al., 2023a); during summer and autumn MBO is also impacted by ozone produced from western forest fires, which have become more frequent in recent years (Farley et al., 2022; Jaffe et al., 2022). It has to be noted that the inclusion of 2020 and 2021 in the analysis did not cause any notable variation in the trend values for several sites across the western US (see Table S1), with the effects of the COVID-19 economic downturn on the long-term trends only visible when considering the spring season (Chang et al., 2023a).

Despite their variability when considering different periods for the trend calculation, the trends for the European sites over 2000–2021 showed persistent negative values when compared to previous literature (e.g., Cristofanelli et al., 2020; Christiansen et al., 2022). While the trends for JFJ and SNB remained almost unchanged, CMN showed a larger negative trend with respect to the 1996–2016 trends reported in Cristofanelli et al. (2020), and ZSF showed a higher (i.e., a less negative) value with respect to this reference period. The positive trends in the Southern Hemisphere are in line with the modeled trends reported by Wang et al. (2022) and with the trends obtained from the TCR-2 chemical reanalysis (Miyazaki et al., 2020).

Regarding positive trends, model studies report increases in the tropospheric ozone burden occurring mainly in the free

troposphere (700–250 hPa, see Fiore et al., 2022), while the surface trends tend to be mixed, especially for the extratropical regions in the Northern Hemisphere (see also Miyazaki et al., 2020; Chang et al., 2023a). This is indeed the case for the European and North American sites reported here (see Fig. 2), indicating that surface O_3 trends are often not related to the trends observed in the free troposphere (Gulev et al., 2021), as also reported by Chang et al. (2023a). However, we emphasize that the sites in Fig. 2 only cover a limited portion of the Earth's surface, as we are limited by the available observations, and these results cannot be assumed to be representative of the entire world.

3.2 Quantification of the anomalies

Figure 3 provides a detailed summary of the anomalies for each site, which are grouped by region and ordered by latitude. Figure S4 in the Supplement shows the same anomalies, but in the form of monthly time series, together with the mean anomalies for the different regions. Figure 3 shows widespread persistent negative anomalies affecting most of the sites in 2020 in both spring (March–May, i.e., MAM) and summer (June–August, i.e., JJA). The situation was somewhat similar in 2021, although some sites showed partial O_3 rebounds (e.g., the sites in the western US). A closer look at the mean seasonal differences for the regions is provided in Table 2, while the focus on the spatial distribution of the anomalies (for the sites in North America and western Europe) for 2019, 2020, and 2021 is provided in Figs. S5–S7 of the Supplement.

By analyzing seasonal means of the anomalies, the western US rural (WUS_R) sites experienced persistent negative anomalies for MAM and JJA 2020 (−6 % and −5 %, respectively), as well as for MAM 2021 (−2 %), while JJA 2021 was characterized by a strong positive anomaly (2.8 ppb, 6 %). Late summer 2020 was characterized by the spread of wildfires in the western US (Filonchyk et al., 2022; Jaffe et al., 2022; Peischl et al., 2023; Langford et al., 2023), resulting in positive mean anomalies for August and September 2020 (2.3 and 2.5 ppb, i.e., 5 % and 6 %, respectively) for several sites (see Fig. S6). Without considering August 2020, the JJA 2020 seasonal mean would result in a much more pronounced negative anomaly, i.e., −4.5 ppb (−10 %), giving an indication of the magnitude of the secondary production of O_3 following the spread of wildfires and thus partly influencing the strong negative anomaly that characterized this region following the 2020 COVID-19 economic downturn. As reported by the World Meteorological Organization (2022), the fire season in western North America in 2021 was also very intense, with the annual total estimated emissions ranking in the top one-third of the years 2003–2021, and contributed to widespread air pollution. The emissions produced by the large widespread wildfires that impacted North America in these months can also explain the different patterns in the western US compared to eastern US and Europe (see Fig. 4).

The situation for the four western US sites downwind of polluted areas (WUS_P) was slightly different, with the negative anomalies being larger than those of WUS_R in MAM 2020 (−4.1 ppb, −9 %), and positive anomalies for 2021 (3 % for both MAM and JJA 2021). The mean anomaly in July 2021 is slightly weaker compared to the WUS_R mean due to the negative anomaly at the JOT site (Fig. 4), despite the other stations being heavily impacted by the North American wildfires (the mean, excluding JOT, for JJA 2021 was 2.8 ppb or 5 %).

The sites in the eastern US (EUS) category experienced negative anomalies in 2020 (−4 % and −12 % for MAM and JJA, respectively) and in JJA 2021 (−8 %) and a positive anomaly in MAM 2021 (3 %). It is interesting to note that, in both of the summer seasons, the EUS sites exhibited an opposite structure with respect to WUS_R and WUS_P sites.

The European sites (EUR) were characterized by persistent negative anomalies throughout all of the considered seasons in Table 2. MAM 2020 reported a total negative anomaly (−2.0 ppb, −3 %) but was characterized by an interesting increase in O_3 concentrations in April, with values almost comparable to the 2000–2019 values, for all stations (even HPB at lower elevation registered a positive anomaly for April 2020; see Fig. 3 and Fig. S6 in the Supplement). This feature was previously observed at CMN by Cristofanelli et al. (2021), who reported that these higher O_3 values were possibly attributed to the frequent occurrence of transport from the free troposphere, transport from areas usually not considered sources of anthropogenic pollution (i.e., the Mediterranean Sea or northern Africa), or the transport of stratospheric air masses. The negative anomalies then continued (except a positive anomaly in June 2021 for HPB, SNB, and ZSF) until September 2021, when all EUR sites experienced a rebound in O_3 values and registered positive anomalies until the end of the year.

While Table 2 reports mean values for the "other" (OT) sites, a consistent "global" picture cannot be drawn, as these sites behaved very differently from each other (see Fig. 3). The SUM (and, partly, IZO) anomalies are more in line with the EUR sites, while DEN, MLO, MKN, and TLL had alternating positive and negative anomalies. PDI showed by far the largest negative anomalies in the first half of 2020 (mean of −8.3 ppb from January to October, −20 %), but unfortunately no information on possible O_3 recovery in 2021 is available due to missing data. The distant Antarctic sites, on the other hand, did not reveal any signal of influence from the COVID-19 economic downturn, with O_3 values perfectly in line with or even higher than the climatological means for both DCC and SPO. For more details about the interannual variability at each site, please refer to Figs. S8–S48 in the Supplement.

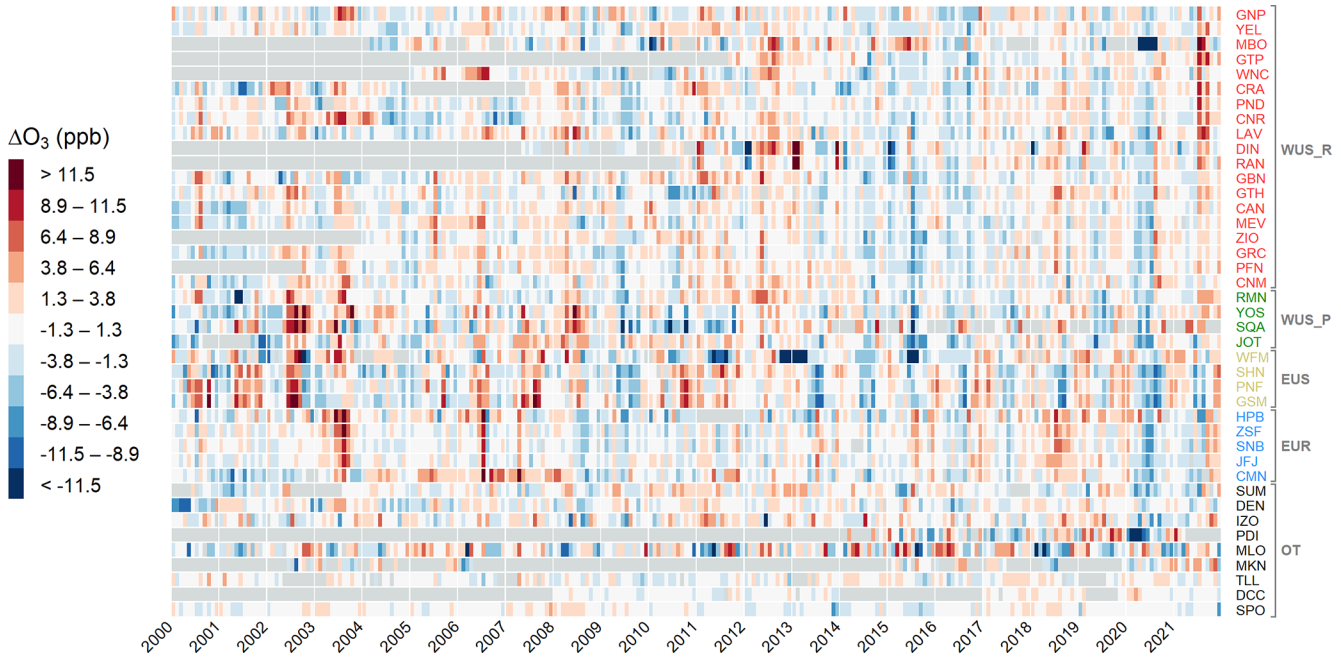

Figure 3. Heatmap of the monthly O_3 anomalies (ΔO_3) for the sites used in this study. The sites are grouped by region (i.e., EUR – Europe, WUS_R – western US "rural", WUS_P – western US "polluted", EUS – eastern US, OT – other) and ordered by decreasing latitude.

Table 2. Seasonal mean anomalies for the different regions considered in this study. Values in brackets indicate percentage variations. The region abbreviations are as follows: WUS_R – western US "rural", WUS_P – western US "polluted", EUS – eastern US, EUR – Europe, OT – other.

Season	WUS_R	WUS_P	EUS	EUR	OT
MAM 2020	−3.1 ppb (−6 %)	−4.3 ppb (−9 %)	−2.5 ppb (−4 %)	−2.1 ppb (−3 %)	−2.1 ppb (−3 %)
JJA 2020	−2.3 ppb (−5 %)	−2.9 ppb (−4 %)	−5.6 ppb (−12 %)	−4.8 ppb (−8 %)	−1.5 ppb (−5 %)
MAM 2021	−0.9 ppb (−2 %)	0.4 ppb (3 %)	0.9 ppb (3 %)	−2.7 ppb (−4 %)	−1.3 ppb (−1 %)
JJA 2021	2.7 ppb (6 %)	1.2 ppb (3 %)	−3.8 ppb (−8 %)	−2.6 ppb (−5 %)	0.4 ppb (1 %)

3.3 Anomaly attribution

The results presented in Sect. 3.2 are in line with those reported in Ziemke et al. (2022), who observed reduced values of tropospheric column ozone (TCO) in spring–summer 2020 and 2021 and who attributed the decrease to reduced pollution (i.e., reductions of ∼ 10 %–20 % in tropospheric NO_2 in the Northern Hemisphere). More specifically, Ziemke et al. (2022) indicate a reduction of 3 Dobson units of TCO, corresponding to a ∼ 7 %–8 % decrease for the area 20° N–60° N. If we consider the seasonal means, excluding the OT category, we obtain almost comparable results for 2020 for the surface O_3 observations (mean negative anomalies of −6 % and −7 % for MAM and JJA, respectively). The situation is different in 2021, for which we obtain higher values (0 % for MAM and −6 % for JJA if we consider EUS and EUR only to exclude wildfire influence). However, it has to be noted that we considered only a selection of sites and that in some cases our seasonal means can be determined by a combination of sub-seasonal positive and negative anomalies (see Sect. 3.2), possibly due to the impact of other "local" factors.

As 2020 was characterized by an unusual stratospheric O_3 depletion event over the Arctic (Dunn et al., 2021), we investigated the possible role of the reduced stratospheric input in O_3 concentrations measured at the high-elevation sites. The minimum in the total column O_3 was observed in March 2020, and this value rapidly recovered in the following months (e.g., Dunn et al., 2021; Chang et al., 2022). The effects of this O_3 depletion on the anomalies were also analyzed by Steinbrecht et al. (2021), and simulations from the NASA GMI model indicated that this depletion contributed to less than one-quarter of the observed anomalies in the troposphere. Moreover, Ziemke et al. (2022) indicate that the observed reduction in stratosphere-to-troposphere exchange (STE) in 2020 did not drive the anomalies in the free troposphere, as NASA satellite measurements showed negative tropospheric O_3 anomalies in both 2020 and 2021, whereas the meteorological conditions controlling the strength of STE

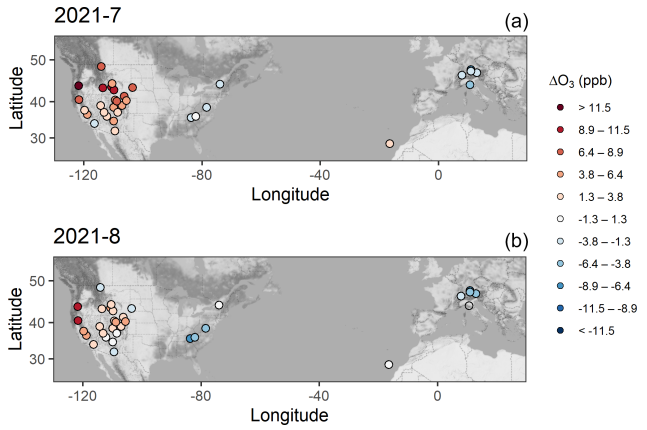

Figure 4. Spatial distribution of the anomalies (ΔO_3) for July **(a)** and August **(b)** 2021, for sites in North America and western Europe. The full series of monthly maps for 2019, 2020, and 2021 is provided in the Supplement (Figs. S5–S7).

were close to the climatological means in 2021; thus, they suggested that the tropospheric anomalies can be largely attributed to decreases in emissions. This was further confirmed by our results: Table 2 shows that most of the regions considered in this study showed the largest O_3 anomalies in JJA 2020 rather than MAM 2020. Therefore, we hypothesize that the reduction in the stratosphere-to-troposphere transport that occurred in 2020 could have played only a minor role in modulating the O_3 anomalies.

3.3.1 Column O_3 variability from IASI

Reductions in mid-tropospheric O_3 seen by the IASI satellite instrument are similar to the ones from the surface observations. Figure 5 shows the 2008–2020 variability of O_3 in the 3–6 km column (both monthly means and anomalies) for three specific regions: (i) an area around the European Alpine sites (i.e., EUR, 40–50° N, 5–20° E), (ii) the eastern US (EUS, 35–50° N, 85–70° W), and (iii) the western US (WUS, 30–50° N, 125–100° W). As stated in Sect. 2.2, the 3–6 km column corresponds to the maximum sensitivity of the IASI retrieval in the free troposphere and is, thus, superior to the 0–3 km column, where the retrieval sensitivity is more limited and the column is not independent of the column above. We did not include 2021 in the analysis as IASI-A operations stopped before the end of the year and all the measurements were not done in the nominal mode of the satellite and the instrument.

In all three regions reductions in the 3–6 km column O_3 were observed in 2020 for both the monthly means and the anomalies. Mean negative anomalies were continuously observed throughout MAM and JJA 2020. The anomalies in MAM 2020 were quite similar among the regions, i.e., −3 % for EUS, −4 % for EUR, and −5 % for WUS. A similar anomaly (−6 %) was also observed for WUS in JJA 2020, and these negative values also persisted in fall (SON), indicating that the wildfire influence had only a minor impact at this upper layer with respect to the surface monitoring sites. For both EUR and EUS, negative anomalies were still observed in JJA 2020 (−1 % and −7 %, respectively), and a rebound occurred in SON, with values falling within 1 standard deviation of the 2008–2019 climatological mean. The smaller EUR anomaly with respect to EUS in JJA 2020 can be explained by the increase in concentrations that characterized the European region in June.

Despite the differences due to the subsets investigated in this study, these results are comparable to the reductions in free-tropospheric O_3 observed by Steinbrecht et al. (2021), i.e., −7 % (with respect to the 2000–2020 climatological mean) from April to August and for the 1–8 km layer in the Northern Hemisphere. Moreover, the behavior of the anomalies observed here is consistent with the tropospheric O_3 anomalies shown by Miyazaki et al. (2021) and Ziemke et al. (2022) discussed above, including the rebound in SON, resulting in column O_3 values comparable to the previous years. However, it has to be noted that our anomalies are weaker than the ones presented in Ziemke et al. (2022), as we are limiting the IASI measurements to land regions around our measurement sites, while Ziemke et al. (2022) observed the largest negative 2020 and 2021 anomalies above the ocean areas of the Northern Hemisphere.

3.3.2 Emissions reductions

To investigate the reductions in the emissions, we analyzed data from the Carbon Monitor, a near-real-time dataset of global CO_2 emissions from fossil fuels and cement production, available since January 2019 (Liu et al., 2020).

Tables 3 and 4 report the CO_2 global emissions variations from the Carbon Monitor, divided into the different sectors, for the combinations of 2019, 2020, and 2021. As also done above for the characterization of the anomalies, here we consider 2019 to be the reference year for "pre-COVID-19" emissions and 2020 and 2021 to be the ones affected by the COVID-19 economic downturn, with a possible recovery in emissions. By analyzing all sectors together, we can immediately spot the decrease in emissions occurring in 2020 with respect to 2019 (−5.3 %) and the strong rebound of emissions in 2021 (+0.5 % and +6.1 % with respect to 2019 and 2020, respectively). The rebound of emissions near pre-COVID-19 levels was also analyzed in other recent works, indicating that fossil fuel CO_2 emissions in 2021 nearly pushed global emissions back to 2019 levels (Jackson et al., 2022) and that 2021 emissions would have even exceeded the 2019 values if not for several low-income countries that had not recovered from the pandemic yet (Davis et al., 2022).

As the strongest O_3 anomalies presented in this study are clustered in the western US and Europe, we also focused on regional CO_2 anomalies by analyzing the US and Europe values provided by the Carbon Monitor (see Tables S2 and S3

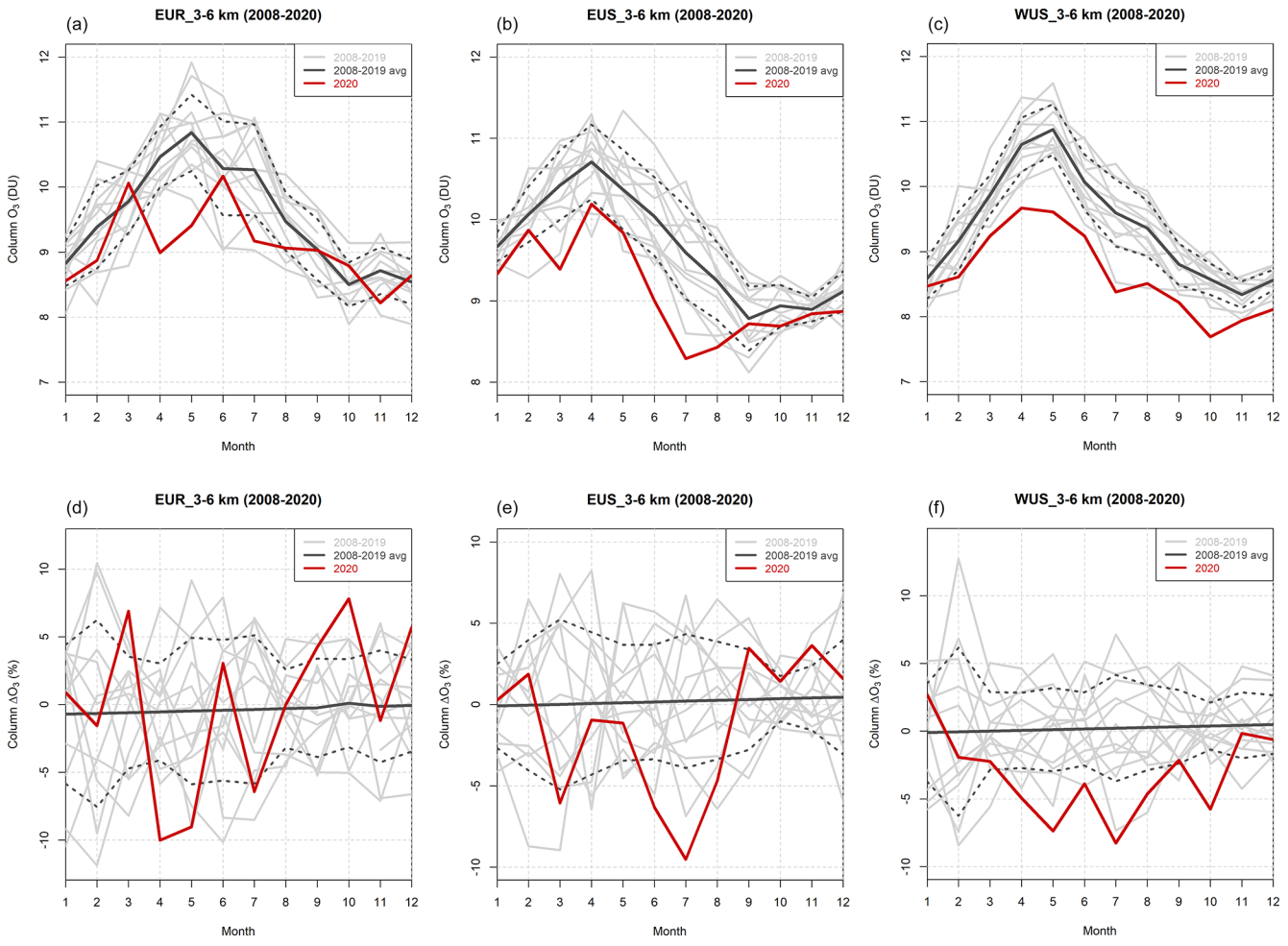

Figure 5. Annual variability of the 3–6 km column O_3 monthly means **(a, b, c)** and anomalies **(d, e, f)** from IASI for the three regions considered (i.e., EUR, EUS, and WUS; for details on definitions refer to Sect. 3.3.1). The gray lines indicate the single years from 2008 to 2019, the black line is the 2008–2019 climatology (together with ± 1 standard deviation, dotted lines), and the red line indicates 2020.

in the Supplement). In this case, no distinction between the western and eastern US is made, and Europe is considered to be composed of the emissions in the 27 European Union countries plus the United Kingdom. While the decrease in 2020 emissions with respect to 2019 was evident for both regions (−10.9 % and −10.1 % for Europe and the US, respectively), the rebound to pre-COVID-19 levels (i.e., 2021 against 2019 emissions) was smaller for these two areas with respect to the global rebound (−2.7 % and −4.5 % for Europe and the US, respectively). This may be one of the causes of the persistent O_3 negative anomalies that still characterized 2021. For Europe, the O_3 negative anomalies that were observed throughout MAM and JJA 2021 could be partly explained by an incomplete recovery in the emissions (−2.9 % and −6.3 % for MAM and JJA, respectively, considering all sectors together). For the US, the CO_2 anomalies are more evident in MAM 2021 (−5.8 %) than in JJA (−0.3 %).

Analyzing the different sectors separately, the limits imposed on domestic and international aviation caused the largest negative variations in 2020 with respect to pre-COVID-19 levels; these sectors witnessed the largest rebounds in 2021, although they did not return to 2019 levels (and this was particularly true for international aviation, where a total difference of −48.3 % and −33.9 % was still observed for Europe and the US, respectively). Particularly for the rural and remote sites, aircraft emissions play a key role in determining the tropospheric O_3 trends, mainly because of the aircraft emitting NO_x in the middle and upper troposphere, where O_3 production efficiency is high (Wang et al., 2022). Therefore, this incomplete recovery in aircraft emissions for 2021 could partly explain the persistent negative anomalies observed. Also, ground transport and, to a lesser extent, residential emissions variations showed the same behavior (while this was true for the global and US emissions, Europe had larger emissions for these two sectors in 2021 with respect to 2019; see Table S2). On a global scale, rebounds in 2021 for power and industry were so large that the emissions in this year exceeded those of 2019 (3.9 %

Table 3. CO_2 global emissions variations (expressed in %) from the Carbon Monitor (Liu et al., 2020) for the different combinations of the years 2019, 2020, and 2021 and with focus on MAM and JJA for each comparison. The percentage represents the contribution of each sector to the total change (i.e., "All sectors").

	2020 vs. 2019			2021 vs. 2019			2021 vs. 2020		
Sector	All	MAM	JJA	All	MAM	JJA	All	MAM	JJA
All sectors	−5.3 %	−13.6 %	−4.0 %	+0.5 %	+0.9 %	+1.5 %	+6.1 %	+16.8 %	+5.7 %
Power	−1.1 %	−3.3 %	+0.0 %	+1.5 %	+1.6 %	+2.7 %	+2.7 %	+5.7 %	+2.9 %
Industry	−0.7 %	−3.3 %	−0.8 %	+0.7 %	+1.3 %	+0.4 %	+1.5 %	+5.4 %	+1.2 %
Ground transport	−2.0 %	−5.0 %	−1.4 %	−0.6 %	−0.8 %	−0.5 %	+1.5 %	+4.8 %	+0.9 %
Residential	−0.2 %	−0.3 %	+0.1 %	−0.1 %	−0.1 %	+0.0 %	+0.0 %	+0.2 %	+0.0 %
Domestic aviation	−0.3 %	−0.5 %	−0.4 %	−0.1 %	−0.1 %	−0.1 %	+0.2 %	+0.4 %	+0.3 %
International aviation	−1.0 %	−1.2 %	−1.5 %	−0.9 %	−1.0 %	−1.0 %	+0.1 %	+0.2 %	+0.5 %

and 2.2 % for power and industry, respectively); on the other hand, positive emissions anomalies in these two sectors were observed for European industry emissions only, with negative emissions observed in the US and for the power sector for both regions.

3.4 Possible O_3 recovery in 2022

The data presented in this study concerned the first full year after the 2020 COVID-19 economic downturn (i.e., ending in December 2021), and therefore little information on the possible recovery of O_3 values to pre-COVID-19 levels is present. Nevertheless, the datasets discussed here are to date the most comprehensive time series for investigating these anomalies from high-elevation stations. The availability of validated 2022 data for the four mountaintop WMO/GAW global stations in Europe (i.e., CMN, SNB, ZSF, and JFJ) allowed us to investigate the possible rebound of O_3 values for this specific European area that encompasses the Alps and the northern Apennines (see Fig. 6). In this case, the monthly data were again detrended before the calculation of the anomalies, but with respect to the whole 2000–2022 period; the reference for the calculation of the climatology was still the 2000–2019 period.

At all four sites, the negative 2000–2019 trends became increasingly more negative when including the 2020 and 2021 data (see Sect. 3.1 and Table S1). But the inclusion of the 2022 data slightly shifted the trends back towards the pre-pandemic levels, i.e., −2.35 ppb per decade (± 1.53 ppb per decade, $p < 0.01$) for CMN, −1.34 ppb per decade (± 0.74 ppb per decade, $p < 0.01$) for SNB, −0.52 ppb per decade (± 0.77 ppb per decade, $p = 0.18$) for ZSF, and −0.64 ppb per decade (± 1.04, $p = 0.22$) for JFJ.

When looking at monthly O_3 values and anomalies (Fig. 6), an overall rebound for 2022 seems evident in the first part of the year (January to March) for all four sites, with monthly means comparable to the climatology, while the anomalies from April to June showed negative values. The values for the rest of the year were generally within 1 standard deviation of the climatological means, with 2 months (July and August) exhibiting higher monthly means with respect to the 2000–2019 baseline. The characteristics of the O_3 rebound in 2022, which are commonly shared among the high-elevation sites located in western Europe, will certainly need deeper investigation, especially for the attribution of the lower values observed from April to June, given that no restrictions driving the variability of the O_3 precursors were present in 2022. Other than meteorological variations, mineral dust transport has been proven to significantly reduce the O_3 values at these high-elevation sites (e.g., Duchi et al., 2016). As the first half of 2022 was largely affected by Saharan mineral dust transport events reaching western Europe (in both March and June 2022), these could have played an important role in lowering the O_3 values in this period.

4 Conclusions

In this paper we demonstrated that the negative O_3 anomalies that were observed in the free troposphere in recent studies also occurred in the boundary layer surrounding several high-elevation sites. This was done by investigating the surface O_3 variability at 41 regionally distributed high-elevation sites following the COVID-19 economic downturn that occurred in 2020 and the following year of 2021, associated with a recovery of emissions. Widespread persistent negative anomalies were observed both in spring (MAM) and summer (JJA) 2020 for all of the regions considered in this study, while for 2021 continuous negative anomalies throughout MAM and JJA were observed only for Europe and, partially, for the eastern US. On the other hand, the western US sites were heavily impacted by wildfire emissions in 2021, resulting in positive anomalies, especially for JJA and for the rural sites. A global picture for the rest of the world could not be drawn, as the sites span a range of different environments and did not show consistent patterns.

The anomaly behavior was further studied by analyzing the variability in the column O_3 from the IASI satellite products. Consistent with previous studies (e.g., Miyazaki et al.,

Table 4. Same as Table 3, but in this case the percentage indicates the sector change in the selected year with respect to the comparison year.

	2020 vs. 2019			2021 vs. 2019			2021 vs. 2020		
Sector	All	MAM	JJA	All	MAM	JJA	All	MAM	JJA
Power	−2.8 %	−9.0 %	−0.1 %	3.9 %	4.3 %	6.7 %	6.9 %	14.7 %	6.8 %
Industry	−2.5 %	−10.6 %	−2.4 %	2.2 %	4.2 %	1.1 %	4.9 %	16.5 %	3.6 %
Ground transport	−10.9 %	−26.1 %	−7.3 %	−3.1 %	−4.2 %	−2.7 %	8.8 %	29.6 %	4.9 %
Residential	−1.6 %	−2.9 %	1.0 %	−1.2 %	−0.9 %	0.2 %	0.4 %	2.1 %	−0.8 %
Domestic aviation	−30.8 %	−49.6 %	−38.0 %	−13.1 %	−11.9 %	−10.3 %	25.5 %	74.7 %	44.5 %
International aviation	−56.0 %	−67.0 %	−71.2 %	−48.2 %	−58.5 %	−48.0 %	17.7 %	25.5 %	80.2 %

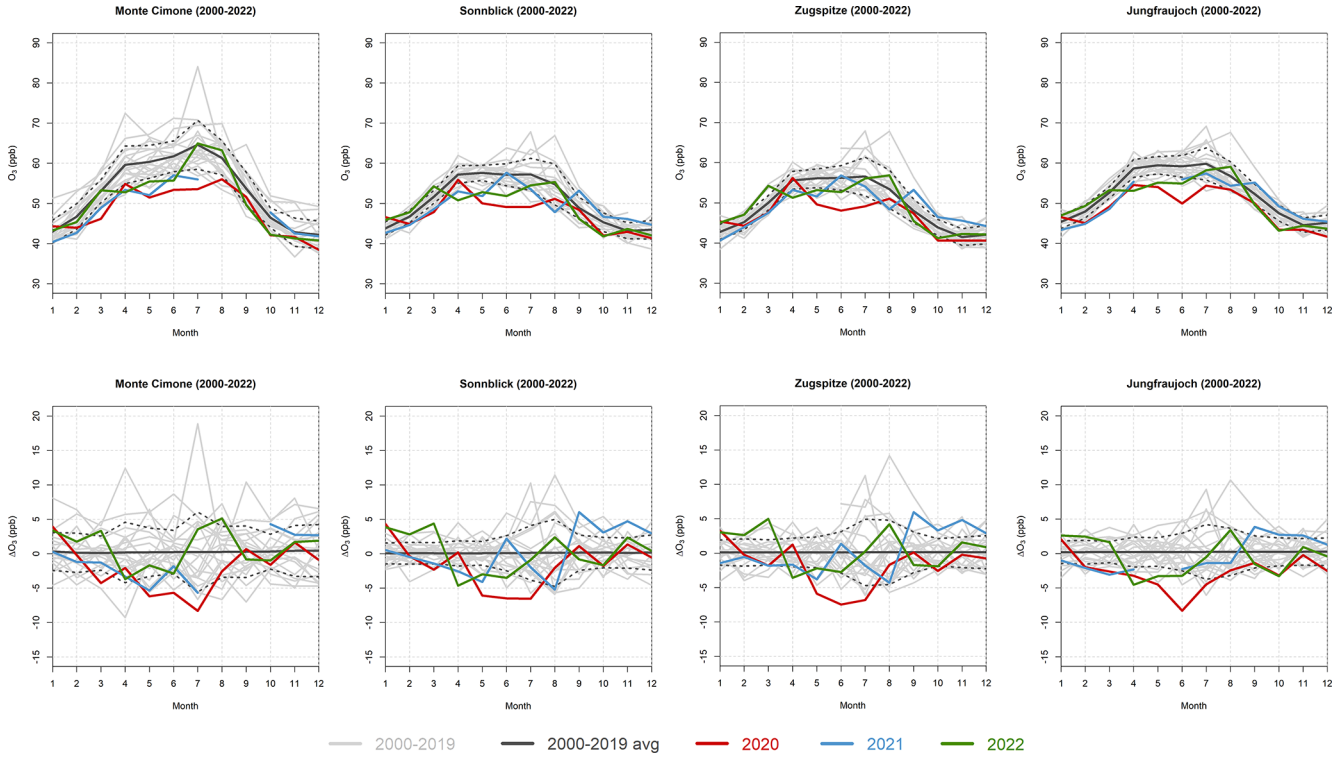

Figure 6. Annual variability of the O_3 monthly means (top row) and anomalies (bottom row) at CMN, SNB, ZSF, and JFJ. The gray lines indicate the single years from 2000 to 2019, the black line is the 2000–2019 climatology (together with ± 1 standard deviation, dotted lines), and the red, blue, and green lines indicate 2020, 2021, and 2022, respectively.

2021; Ziemke et al., 2022), negative anomalies were also observed in the free-tropospheric 3–6 km column O_3 product for both MAM and JJA 2020 (−4 % for both seasons on average over the considered regions). These results indicate that one of the causes of such widespread anomalies is the reduction in the emissions of the O_3 precursors. To further assess this point, we also investigated the reduction in the emissions for the different sectors for the years 2019, 2020, and 2021, as derived from the Carbon Monitor, a near-real-time dataset of global CO_2 emissions. The results highlight the decrease in emissions that occurred in 2020 with respect to 2019 (−10.9 % and −10.1 % analyzing all sectors together for both Europe and the US, respectively) and the rebound of emissions in 2021 that took place globally. However, the recovery in emissions in 2021 did not reach "pre-COVID-19" levels of 2019 in the two macro-regions that encompass most of the sites investigated here (−2.7 % and −4.5 % for Europe and the US, respectively), and this could be one of the causes of the persistent negative anomalies that were observed in these two areas.

As our dataset was limited to the first full year after the 2020 COVID-19 economic downturn, few conclusions could be drawn regarding the full recovery of O_3 values to pre-COVID-19 levels. However, we made use of 2022 data for four mountaintop sites in western Europe, and we observed a common pattern concerning O_3 variability in 2022. This was characterized by a rebound in the first part of the year (January to March), with monthly values comparable to the

2000–2019 climatology; then, from April to June negative anomalies were observed, and the values for the remaining part of the year were within 1 standard deviation of the climatological averages. The rebound in O_3 values starting from 2021–2022 will certainly need deeper investigation, especially concerning the attribution of the wide-ranging variability, and will be the subject of future research.

Data availability. The ozone data for CMN, DCC, HPB, IZO, JFJ, MLO, MKN, PDI, SNB, SPO, SUM, TLL, and ZSF stations can be retrieved from the WMO/GAW World Data Center for Reactive Gases (WDCRG) hosted by NILU (https://ebas.nilu.no/, EBAS, 2023). Data for MBO are permanently archived by the University of Washington in its ResearchWorks archive; see https://sites.uw.edu/jaffe-group/mt-bachelor-observatory/ (University of Washington, 2023). The Clean Air Status and Trends Network (CASTNET) ozone data can be retrieved at https://www.epa.gov/castnet (CASTNET, 2023). Carbon Monitor data were downloaded from https://carbonmonitor.org/ (Carbon Monitor, 2023) and the data presented in this study refer to the 30 April 2023 data update. The IASI dataset can be retrieved at https://doi.org/10.14768/52460ee0-30d3-4c89-8a01-888966d68087 (Dufour and Eremenko, 2023).

Supplement. The supplement related to this article is available online at: https://doi.org/10.5194/acp-23-15693-2023-supplement.

Author contributions. DP, PC, and ORC contributed to the conception and design of the study. DP conducted the data analysis with inputs from ORC, PC, and KLC. GD contributed the IASI data and advised on their interpretation. GB, CC, PE, DJ, DK, JL, IP, MP, TS, BCS, MS, CT, and PC provided the ozone measurements. DP drafted the paper with inputs from ORC, PC, KLC, and GD. All authors contributed to the discussion and improvement of the paper.

Competing interests. ORC is the Scientific Coordinator of the TOAR-II Community Special Issue, to which this paper has been submitted, but he is not involved with the anonymous peer-review process of this or any of the other papers submitted to the special issue journals.

Disclaimer. Publisher's note: Copernicus Publications remains neutral with regard to jurisdictional claims made in the text, published maps, institutional affiliations, or any other geographical representation in this paper. While Copernicus Publications makes every effort to include appropriate place names, the final responsibility lies with the authors.

Special issue statement. This article is part of the special issue "Tropospheric Ozone Assessment Report Phase II (TOAR-II) Community Special Issue (ACP/AMT/BG/GMD inter-journal SI)". It is a result of the Tropospheric Ozone Assessment Report, Phase II (TOAR-II, 2020–2024).

Acknowledgements. We would like to thank Iris Buxbaum and Wolfgang Spangl at the Umweltbundesamt/Federal Environment Agency, Austria, for providing the Sonnblick data; the Dirección Meteorológica de Chile for providing data from El Tololo, Chile; the Kenya Meteorological Department for providing data from Mt. Kenya, Kenya; the Vietnam National Centre for Hydro-Meteorological Forecasting for providing data from Pha Din, Vietnam; and Robert Holla at the Deutscher Wetterdienst/German Meteorological Service for providing data from Hohenpeißenberg, Germany. The ozone measurements at Concordia, Antarctica, were carried out during several Italian Antarctic Research Programme (PNRA) projects, such as "LTCPAA – Long-term Measurements of Chemical and Physical Properties of Atmospheric Aerosol at Dome C" and "STEAR – Stratosphere-to-Troposphere Exchange in the Antarctic Region", and the authors thank the joint French–Italian Concordia Program and the logistics team (IPEV-PNRA) for their kind assistance during the experimental campaigns. We would also like to thank Rodrigo Seguel and two anonymous referees for their valuable and constructive feedback on our paper.

Financial support. The research leading to these results has received funding from the European Union's Horizon 2020 research and innovation program (grant agreement no. 654109). Surface O_3 measurements at Summit are made possible via the US National Science Foundation Office of Polar Programs and their contract with Battelle Arctic Research Operations (contract no. 49100420C0001). Owen R. Cooper, Kai-Lan Chang, Irina Petropavlovskikh, and Peter Effertz were supported by a NOAA cooperative agreement (grant no. NA22OAR4320151). The publication costs of this research have been partially supported by the European Commission under the Horizon 2020 research and innovation framework program through ACTMO-ACCESS Integrating Activity (grant agreement no. 101008004).

Review statement. This paper was edited by Tao Wang and reviewed by two anonymous referees.

References

Adam, M. G., Tran, P. T., and Balasubramanian, R.: Air quality changes in cities during the COVID-19 lockdown: A critical review, Atmos. Res., 264, 105823, https://doi.org/10.1016/j.atmosres.2021.105823, 2021.

Bouarar, I., Gaubert, B., Brasseur, G. P., Steinbrecht, W., Doumbia, T., Tilmes, S., Liu, Y., Stavrakou, T., Deroubaix, A., Darras, S., Granier, C., Lacey, F., Müller, J.-F., Shi, X., Elguindi, N., and Wang, T.: Ozone Anomalies in the Free Troposphere During the COVID-19 Pandemic, Geophys. Res. Lett., 48, e2021GL094204, https://doi.org/10.1029/2021GL094204, 2021.

Carbon Monitor: Carbon Monitor, https://carbonmonitor.org/ (last access: 11 May 2023), 2023.

CASTNET: Clean Air Status and Trends Network (CASTNET), https://www.epa.gov/castnet (last access: 11 August 2022), 2023.

Chang, K.-L., Schultz, M. G., Lan, X., McClure-Begley, A., Petropavlovskikh, I., Xu, X., and Ziemke, J. R.: Trend detection of atmospheric time series: Incorporating appropriate uncertainty

estimates and handling extreme events, Elementa: Science of the Anthropocene, 9, https://doi.org/10.1525/elementa.2021.00035, 00035, 2021.

Chang, K.-L., Cooper, O. R., Gaudel, A., Allaart, M., Ancellet, G., Clark, H., Godin-Beekmann, S., Leblanc, T., Van Malderen, R., Nédélec, P., Petropavlovskikh, I., Steinbrecht, W., Stübi, R., Tarasick, D. W., and Torres, C.: Impact of the COVID-19 economic downturn on tropospheric ozone trends: an uncertainty weighted data synthesis for quantifying regional anomalies above Western North America and Europe, AGU Advances, 3, e2021AV000542, https://doi.org/10.1029/2021AV000542, 2022.

Chang, K.-L., Cooper, O. R., Rodriguez, G., Iraci, L. T., Yates, E. L., Johnson, M. S., Gaudel, A., Jaffe, D. A., Bernays, N., Clark, H., Effertz, P., Leblanc, T., Petropavlovskikh, I., Sauvage, B., and Tarasick, D. W.: Diverging Ozone Trends Above Western North America: Boundary Layer Decreases Versus Free Tropospheric Increases, J. Geophys. Res.-Atmos., 128, e2022JD038090, https://doi.org/10.1029/2022JD038090, 2023a.

Chang, K.-L., Schultz, M. G., Koren, G., and Selke, N.: Guidance note on best statistical practices for TOAR analyses, Cornell University, https://doi.org/10.48550/arXiv.2304.14236, 2023b.

Chossière, G. P., Xu, H., Dixit, Y., Isaacs, S., Eastham, S. D., Allroggen, F., Speth, R. L., and Barrett, S. R. H.: Air pollution impacts of COVID-19-related containment measures, Sci. Adv., 7, eabe1178, https://doi.org/10.1126/sciadv.abe1178, 2021.

Christiansen, A., Mickley, L. J., Liu, J., Oman, L. D., and Hu, L.: Multidecadal increases in global tropospheric ozone derived from ozonesonde and surface site observations: can models reproduce ozone trends?, Atmos. Chem. Phys., 22, 14751–14782, https://doi.org/10.5194/acp-22-14751-2022, 2022.

Clark, H., Bennouna, Y., Tsivlidou, M., Wolff, P., Sauvage, B., Barret, B., Le Flochmoën, E., Blot, R., Boulanger, D., Cousin, J.-M., Nédélec, P., Petzold, A., and Thouret, V.: The effects of the COVID-19 lockdowns on the composition of the troposphere as seen by In-service Aircraft for a Global Observing System (IAGOS) at Frankfurt, Atmos. Chem. Phys., 21, 16237–16256, https://doi.org/10.5194/acp-21-16237-2021, 2021.

Clerbaux, C., Boynard, A., Clarisse, L., George, M., Hadji-Lazaro, J., Herbin, H., Hurtmans, D., Pommier, M., Razavi, A., Turquety, S., Wespes, C., and Coheur, P.-F.: Monitoring of atmospheric composition using the thermal infrared IASI/MetOp sounder, Atmos. Chem. Phys., 9, 6041–6054, https://doi.org/10.5194/acp-9-6041-2009, 2009.

Cooper, O. R., Schultz, M. G., Schröder, S., Chang, K.-L., Gaudel, A., Benítez, G. C., Cuevas, E., Fröhlich, M., Galbally, I. E., Molloy, S., Kubistin, D., Lu, X., McClure-Begley, A., Nédélec, P., O'Brien, J., Oltmans, S. J., Petropavlovskikh, I., Ries, L., Senik, I., Sjöberg, K., Solberg, S., Spain, G. T., Spangl, W., Steinbacher, M., Tarasick, D., Thouret, V., and Xu, X.: Multi-decadal surface ozone trends at globally distributed remote locations, Elementa: Science of the Anthropocene, 8, 23, https://doi.org/10.1525/elementa.420, 2020.

Cristofanelli, P., Fierli, F., Graziosi, F., Steinbacher, M., Couret, C., Calzolari, F., Roccato, F., Landi, T., Putero, D., and Bonasoni, P.: Decadal O_3 variability at the Mt. Cimone WMO/GAW global station (2,165 m a.s.l., Italy) and comparison with two high-mountain "reference" sites in Europe, Elementa: Science of the Anthropocene, 8, 00042, https://doi.org/10.1525/elementa.00042, 2020.

Cristofanelli, P., Arduni, J., Serva, F., Calzolari, F., Bonasoni, P., Busetto, M., Maione, M., Sprenger, M., Trisolino, P., and Putero, D.: Negative ozone anomalies at a high mountain site in northern Italy during 2020: a possible role of COVID-19 lockdowns?, Environ. Res. Lett., 16, 074029, https://doi.org/10.1088/1748-9326/ac0b6a, 2021.

Cuesta, J., Costantino, L., Beekmann, M., Siour, G., Menut, L., Bessagnet, B., Landi, T. C., Dufour, G., and Eremenko, M.: Ozone pollution during the COVID-19 lockdown in the spring of 2020 over Europe, analysed from satellite observations, in situ measurements, and models, Atmos. Chem. Phys., 22, 4471–4489, https://doi.org/10.5194/acp-22-4471-2022, 2022.

Davis, S. J., Liu, Z., Deng, Z., Zhu, B., Ke, P., Sun, T., Guo, R., Hong, C., Zheng, B., Wang, Y., Boucher, O., Gentine, P., and Ciais, P.: Emissions rebound from the COVID-19 pandemic, Nat. Clim. Change, 12, 412–414, https://doi.org/10.1038/s41558-022-01332-6, 2022.

Duchi, R., Cristofanelli, P., Landi, T. C., Arduini, J., Bonafè, U., Bourcier, L., Busetto, M., Calzolari, F., Marinoni, A., Putero, D., and Bonasoni, P.: Long-term (2002–2012) investigation of Saharan dust transport events at Mt. Cimone GAW global station, Italy (2165 m a.s.l.), Elementa: Science of the Anthropocene, 4, 000085, https://doi.org/10.12952/journal.elementa.000085, 2016.

Dufour, G. and Eremenko, M.: IASI monthly O3 partial columns over European, Eastern US and Western US Mountains between 2008 and 2020, IPSL Data Catalog [data set], https://doi.org/10.14768/52460ee0-30d3-4c89-8a01-888966d68087, 2023.

Dufour, G., Eremenko, M., Orphal, J., and Flaud, J.-M.: IASI observations of seasonal and day-to-day variations of tropospheric ozone over three highly populated areas of China: Beijing, Shanghai, and Hong Kong, Atmos. Chem. Phys., 10, 3787–3801, https://doi.org/10.5194/acp-10-3787-2010, 2010.

Dufour, G., Eremenko, M., Griesfeller, A., Barret, B., LeFlochmoën, E., Clerbaux, C., Hadji-Lazaro, J., Coheur, P.-F., and Hurtmans, D.: Validation of three different scientific ozone products retrieved from IASI spectra using ozonesondes, Atmos. Meas. Tech., 5, 611–630, https://doi.org/10.5194/amt-5-611-2012, 2012.

Dufour, G., Hauglustaine, D., Zhang, Y., Eremenko, M., Cohen, Y., Gaudel, A., Siour, G., Lachatre, M., Bense, A., Bessagnet, B., Cuesta, J., Ziemke, J., Thouret, V., and Zheng, B.: Recent ozone trends in the Chinese free troposphere: role of the local emission reductions and meteorology, Atmos. Chem. Phys., 21, 16001–16025, https://doi.org/10.5194/acp-21-16001-2021, 2021.

Dunn, R. J. H., Alfred, F., Gobron, N., Miller, J. B., and Willett, K. M.: Global Climate [in "State of the Climate in 2020"], B. Am. Meteorol. Soc., 102, S11–S141, https://doi.org/10.1175/BAMS-D-21-0098.1, 2021.

EBAS: EBAS Home, https://ebas.nilu.no/ (last access: 24 October 2022), 2023.

Eremenko, M., Dufour, G., Foret, G., Keim, C., Orphal, J., Beekmann, M., Bergametti, G., and Flaud, J.-M.: Tropospheric ozone distributions over Europe during the heat wave in July 2007 observed from infrared nadir spectra recorded by IASI, Geophys. Res. Lett., 35, L18805, https://doi.org/10.1029/2008GL034803, 2008.

Farley, R., Bernays, N., Jaffe, D. A., Ketcherside, D., Hu, L., Zhou, S., Collier, S., and Zhang, Q.: Persistent Influence of Wildfire Emissions in the Western United States and Characteristics of Aged Biomass Burning Organic Aerosols under Clean Air Conditions, Environ. Sci. Technol., 56, 3645–3657, https://doi.org/10.1021/acs.est.1c07301, pMID: 35229595, 2022.

Filonchyk, M., Peterson, M. P., and Sun, D.: Deterioration of air quality associated with the 2020 US wildfires, Sci. Total Environ., 826, 154103, https://doi.org/10.1016/j.scitotenv.2022.154103, 2022.

Fiore, A. M., Hancock, S. E., Lamarque, J.-F., Correa, G. P., Chang, K.-L., Ru, M., Cooper, O., Gaudel, A., Polvani, L. M., Sauvage, B., and Ziemke, J. R.: Understanding recent tropospheric ozone trends in the context of large internal variability: a new perspective from chemistry-climate model ensembles, Environ. Res.-Clim., 1, 025008, https://doi.org/10.1088/2752-5295/ac9cc2, 2022.

Fleming, Z. L., Doherty, R. M., von Schneidemesser, E., Malley, C. S., Cooper, O. R., Pinto, J. P., Colette, A., Xu, X., Simpson, D., Schultz, M. G., Lefohn, A. S., Hamad, S., Moolla, R., Solberg, S., and Feng, Z.: Tropospheric Ozone Assessment Report: Present-day ozone distribution and trends relevant to human health, Elementa: Science of the Anthropocene, 6, 12, https://doi.org/10.1525/elementa.273, 2018.

Friedlingstein, P., O'Sullivan, M., Jones, M. W., Andrew, R. M., Gregor, L., Hauck, J., Le Quéré, C., Luijkx, I. T., Olsen, A., Peters, G. P., Peters, W., Pongratz, J., Schwingshackl, C., Sitch, S., Canadell, J. G., Ciais, P., Jackson, R. B., Alin, S. R., Alkama, R., Arneth, A., Arora, V. K., Bates, N. R., Becker, M., Bellouin, N., Bittig, H. C., Bopp, L., Chevallier, F., Chini, L. P., Cronin, M., Evans, W., Falk, S., Feely, R. A., Gasser, T., Gehlen, M., Gkritzalis, T., Gloege, L., Grassi, G., Gruber, N., Gürses, Ö., Harris, I., Hefner, M., Houghton, R. A., Hurtt, G. C., Iida, Y., Ilyina, T., Jain, A. K., Jersild, A., Kadono, K., Kato, E., Kennedy, D., Klein Goldewijk, K., Knauer, J., Korsbakken, J. I., Landschützer, P., Lefèvre, N., Lindsay, K., Liu, J., Liu, Z., Marland, G., Mayot, N., McGrath, M. J., Metzl, N., Monacci, N. M., Munro, D. R., Nakaoka, S.-I., Niwa, Y., O'Brien, K., Ono, T., Palmer, P. I., Pan, N., Pierrot, D., Pocock, K., Poulter, B., Resplandy, L., Robertson, E., Rödenbeck, C., Rodriguez, C., Rosan, T. M., Schwinger, J., Séférian, R., Shutler, J. D., Skjelvan, I., Steinhoff, T., Sun, Q., Sutton, A. J., Sweeney, C., Takao, S., Tanhua, T., Tans, P. P., Tian, X., Tian, H., Tilbrook, B., Tsujino, H., Tubiello, F., van der Werf, G. R., Walker, A. P., Wanninkhof, R., Whitehead, C., Willstrand Wranne, A., Wright, R., Yuan, W., Yue, C., Yue, X., Zaehle, S., Zeng, J., and Zheng, B.: Global Carbon Budget 2022, Earth Syst. Sci. Data, 14, 4811–4900, https://doi.org/10.5194/essd-14-4811-2022, 2022.

Galbally, I., Schultz, M., Buchmann, B., Gilge, S., Guenther, F., Koide, H., Oltmans, S., Patrick, L., Scheel, H.-E., Smit, H., Steinbacher, M., Steinbrecht, W., Tarasova, O., Viallon, J., Volz-Thomas, A., Weber, M., Wielgosz, R., and Zellweger, C.: Guidelines for continuous measurements of ozone in the troposphere, GAW Report 209, Publication WMO-No. 1110, WMO, Geneva, Switzerland, 82 pp., https://library.wmo.int/idurl/4/49557 (last acces: 17 April 2023), 2013.

Gaubert, B., Bouarar, I., Doumbia, T., Liu, Y., Stavrakou, T., Deroubaix, A., Darras, S., Elguindi, N., Granier, C., Lacey, F., Müller, J.-F., Shi, X., Tilmes, S., Wang, T., and Brasseur, G. P.: Global Changes in Secondary Atmospheric Pollutants During the 2020 COVID-19 Pandemic, J. Geophys. Res.-Atmos., 126, e2020JD034213, https://doi.org/10.1029/2020JD034213, 2021.

Gkatzelis, G. I., Gilman, J. B., Brown, S. S., Eskes, H., Gomes, A. R., Lange, A. C., McDonald, B. C., Peischl, J., Petzold, A., Thompson, C. R., and Kiendler-Scharr, A.: The global impacts of COVID-19 lockdowns on urban air pollution: A critical review and recommendations, Elementa: Science of the Anthropocene, 9, 00176, https://doi.org/10.1525/elementa.2021.00176, 2021.

Gulev, S., Thorne, P., Ahn, J., Dentener, F., Domingues, C., Gerland, S., Gong, D., Kaufman, D., Nnamchi, H., Quaas, J., Rivera, J., Sathyendranath, S., Smith, S., Trewin, B., von Schuckmann, K., and Vose, R.: Changing State of the Climate System, in: Climate Change 2021: The Physical Science Basis. Contribution of Working Group I to the Sixth Assessment Report of the Intergovernmental Panel on Climate Change, edited by: Masson-Delmotte, V., Zhai, P., Pirani, A., Connors, S. L., Péan, C., Berger, S., Caud, N., Chen, Y., Goldfarb, L., Gomis, M. I., Huang, M., Leitzell, K., Lonnoy, E., Matthews, J. B. R., Maycock, T. K., Waterfield, T., Yelekçi, O., Yu, R., and Zhou, B., book Sect. 2, Cambridge University Press, Cambridge, UK and New York, NY, USA, https://doi.org/10.1017/9781009157896.004, 2021.

Jackson, R. B., Friedlingstein, P., Quéré, C. L., Abernethy, S., Andrew, R. M., Canadell, J. G., Ciais, P., Davis, S. J., Deng, Z., Liu, Z., Korsbakken, J. I., and Peters, G. P.: Global fossil carbon emissions rebound near pre-COVID-19 levels, Environ. Res. Lett., 17, 031001, https://doi.org/10.1088/1748-9326/ac55b6, 2022.

Jaffe, D. A., Ninneman, M., and Chan, H. C.: NO_x and O_3 Trends at U.S. Non-Attainment Areas for 1995–2020: Influence of COVID-19 Reductions and Wildland Fires on Policy-Relevant Concentrations, J. Geophys. Res.-Atmos., 127, e2021JD036385, https://doi.org/10.1029/2021JD036385, 2022.

Keller, C. A., Evans, M. J., Knowland, K. E., Hasenkopf, C. A., Modekurty, S., Lucchesi, R. A., Oda, T., Franca, B. B., Mandarino, F. C., Díaz Suárez, M. V., Ryan, R. G., Fakes, L. H., and Pawson, S.: Global impact of COVID-19 restrictions on the surface concentrations of nitrogen dioxide and ozone, Atmos. Chem. Phys., 21, 3555–3592, https://doi.org/10.5194/acp-21-3555-2021, 2021.

Kumar, P., Kuttippurath, J., von der Gathen, P., Petropavlovskikh, I., Johnson, B., McClure-Begley, A., Cristofanelli, P., Bonasoni, P., Barlasina, M. E., and Sánchez, R.: The increasing surface ozone and tropospheric ozone in Antarctica and their possible drivers, Environ. Sci. Technol., 55, 8542–8553, https://doi.org/10.1021/acs.est.0c08491, 2021.

Lahiri, S. N.: Resampling methods for dependent data, Springer, New York, NY, https://doi.org/10.1007/978-1-4757-3803-2, 2003.

Langford, A. O., Senff, C. J., Alvarez II, R. J., Aikin, K. C., Ahmadov, R., Angevine, W. M., Baidar, S., Brewer, W. A., Brown, S. S., James, E. P., McCarty, B. J., Sandberg, S. P., and Zucker, M. L.: Were wildfires responsible for the unusually high surface ozone in Colorado during 2021?, J. Geophys. Res.-Atmos., 128, e2022JD037700, https://doi.org/10.1029/2022JD037700, 2023.

Le Quéré, C., Jackson, R. B., Jones, M. W., Smith, A. J. P., Abernethy, S., Andrew, R. M., De-Gol, A. J., Willis, D. R., Shan, Y., Canadell, J. G., Friedlingstein, P., Creutzig, F., and Peters,

G.: Temporary reduction in daily global CO_2 emissions during the COVID-19 forced confinement, Nat. Clim. Change, 10, 647–653, https://doi.org/10.1038/s41558-020-0797-x, 2020.

Liu, Z., Ciais, P., Deng, Z., Davis, S. J., Zheng, B., Wang, Y., Cui, D., Zhu, B., Dou, X., Ke, P., Sun, T., Guo, R., Boucher, O., Bréon, F.-M., Lu, C., Guo, R., Xue, J., Boucher, E., Tanaka, K., and Chevallier, F.: Carbon Monitor: a near-real-time daily dataset of global CO_2 emission from fossil fuel and cement production, Sci. Data, 7, 392, https://doi.org/10.1038/s41597-020-00708-7, 2020.

Matthias, V., Quante, M., Arndt, J. A., Badeke, R., Fink, L., Petrik, R., Feldner, J., Schwarzkopf, D., Link, E.-M., Ramacher, M. O. P., and Wedemann, R.: The role of emission reductions and the meteorological situation for air quality improvements during the COVID-19 lockdown period in central Europe, Atmos. Chem. Phys., 21, 13931–13971, https://doi.org/10.5194/acp-21-13931-2021, 2021.

Mertens, M., Jöckel, P., Matthes, S., Nützel, M., Grewe, V., and Sausen, R.: COVID-19 induced lower-tropospheric ozone changes, Environ. Res. Lett., 16, 064005, https://doi.org/10.1088/1748-9326/abf191, 2021.

Mills, G., Pleijel, H., Malley, C. S., Sinha, B., Cooper, O. R., Schultz, M. G., Neufeld, H. S., Simpson, D., Sharps, K., Feng, Z., Gerosa, G., Harmens, H., Kobayashi, K., Saxena, P., Paoletti, E., Sinha, V., and Xu, X.: Tropospheric Ozone Assessment Report: Present-day tropospheric ozone distribution and trends relevant to vegetation, Elementa: Science of the Anthropocene, 6, 47, https://doi.org/10.1525/elementa.302, 2018.

Miyazaki, K., Bowman, K., Sekiya, T., Eskes, H., Boersma, F., Worden, H., Livesey, N., Payne, V. H., Sudo, K., Kanaya, Y., Takigawa, M., and Ogochi, K.: Updated tropospheric chemistry reanalysis and emission estimates, TCR-2, for 2005–2018, Earth Syst. Sci. Data, 12, 2223–2259, https://doi.org/10.5194/essd-12-2223-2020, 2020.

Miyazaki, K., Bowman, K., Sekiya, T., Takigawa, M., Neu, J. L., Sudo, K., Osterman, G., and Eskes, H.: Global tropospheric ozone responses to reduced NOx emissions linked to the COVID-19 worldwide lockdowns, Sci. Adv., 7, eabf7460, https://doi.org/10.1126/sciadv.abf7460, 2021.

Monks, P. S., Archibald, A. T., Colette, A., Cooper, O., Coyle, M., Derwent, R., Fowler, D., Granier, C., Law, K. S., Mills, G. E., Stevenson, D. S., Tarasova, O., Thouret, V., von Schneidemesser, E., Sommariva, R., Wild, O., and Williams, M. L.: Tropospheric ozone and its precursors from the urban to the global scale from air quality to short-lived climate forcer, Atmos. Chem. Phys., 15, 8889–8973, https://doi.org/10.5194/acp-15-8889-2015, 2015.

Peischl, J., Aikin, K. C., McDonald, B. C., Harkins, C., Middlebrook, A. M., Langford, A. O., Cooper, O. R., Chang, K.-L., and Brown, S. S.: Quantifying anomalies of air pollutants in 9 U.S. cities during 2020 due to COVID-19 lockdowns and wildfires based on decadal trends, Elementa: Science of the Anthropocene, 11, 00029, https://doi.org/10.1525/elementa.2023.00029, 2023.

Price, S. and Pales, J. C.: Mauna Loa Observatory: the first five years, Mon. Weather Rev., 91, 665–680, https://doi.org/10.1175/1520-0493(1963)091<0665:MLOTFF>2.3.CO;2, 1963.

Sicard, P., De Marco, A., Agathokleous, E., Feng, Z., Xu, X., Paoletti, E., Rodriguez, J. J. D., and Calatayud, V.: Amplified ozone pollution in cities during the COVID-19 lockdown, Sci. Total Environ.t, 735, 139542, https://doi.org/10.1016/j.scitotenv.2020.139542, 2020.

Sokhi, R. S., Singh, V., Querol, X., Finardi, S., Targino, A. C., de Fatima Andrade, M., Pavlovic, R., Garland, R. M., Massagué, J., Kong, S., Baklanov, A., Ren, L., Tarasova, O., Carmichael, G., Peuch, V.-H., Anand, V., Arbilla, G., Badali, K., Beig, G., Belalcazar, L. C., Bolignano, A., Brimblecombe, P., Camacho, P., Casallas, A., Charland, J.-P., Choi, J., Chourdakis, E., Coll, I., Collins, M., Cyrys, J., da Silva, C. M., Di Giosa, A. D., Di Leo, A., Ferro, C., Gavidia-Calderon, M., Gayen, A., Ginzburg, A., Godefroy, F., Gonzalez, Y. A., Guevara-Luna, M., Haque, S. M., Havenga, H., Herod, D., Hõrrak, U., Hussein, T., Ibarra, S., Jaimes, M., Kaasik, M., Khaiwal, R., Kim, J., Kousa, A., Kukkonen, J., Kulmala, M., Kuula, J., La Violette, N., Lanzani, G., Liu, X., MacDougall, S., Manseau, P. M., Marchegiani, G., McDonald, B., Mishra, S. V., Molina, L. T., Mooibroek, D., Mor, S., Moussiopoulos, N., Murena, F., Niemi, J. V., Noe, S., Nogueira, T., Norman, M., Pérez-Camaño, J. L., Petäjä, T., Piketh, S., Rathod, A., Reid, K., Retama, A., Rivera, O., Rojas, N. Y., Rojas-Quincho, J. P., San José, R., Sánchez, O., Seguel, R. J., Sillanpää, S., Su, Y., Tapper, N., Terrazas, A., Timonen, H., Toscano, D., Tsegas, G., Velders, G. J., Vlachokostas, C., von Schneidemesser, E., VPM, R., Yadav, R., Zalakeviciute, R., and Zavala, M.: A global observational analysis to understand changes in air quality during exceptionally low anthropogenic emission conditions, Environ. Int., 157, 106818, https://doi.org/10.1016/j.envint.2021.106818, 2021.

Steinbrecht, W., Kubistin, D., Plass-Dülmer, C., Davies, J., Tarasick, D. W., von der Gathen, P., Deckelmann, H., Jepsen, N., Kivi, R., Lyall, N., Palm, M., Notholt, J., Kois, B., Oelsner, P., Allaart, M., Piters, A., Gill, M., Van Malderen, R., Delcloo, A. W., Sussmann, R., Mahieu, E., Servais, C., Romanens, G., Stübi, R., Ancellet, G., Godin-Beekmann, S., Yamanouchi, S., Strong, K., Johnson, B., Cullis, P., Petropavlovskikh, I., Hannigan, J. W., Hernandez, J.-L., Diaz Rodriguez, A., Nakano, T., Chouza, F., Leblanc, T., Torres, C., Garcia, O., Röhling, A. N., Schneider, M., Blumenstock, T., Tully, M., Paton-Walsh, C., Jones, N., Querel, R., Strahan, S., Stauffer, R. M., Thompson, A. M., Inness, A., Engelen, R., Chang, K.-L., and Cooper, O. R.: COVID-19 crisis reduces free tropospheric ozone across the Northern Hemisphere, Geophys. Res. Lett., 48, e2020GL091987, https://doi.org/10.1029/2020GL091987, 2021.

Szopa, S., Naik, V., Adhikary, B., Artaxo, P., Berntsen, T., Collins, W., Fuzzi, S., Gallardo, L., Kiendler-Scharr, A., Klimont, Z., Liao, H., Unger, N., and Zanis, P.: Short-Lived Climate Forcers, in: Climate Change 2021: The Physical Science Basis. Contribution of Working Group I to the Sixth Assessment Report of the Intergovernmental Panel on Climate Change, edited by Masson-Delmotte, V., Zhai, P., Pirani, A., Connors, S. L., Péan, C., Berger, S., Caud, N., Chen, Y., Goldfarb, L., Gomis, M. I., Huang, M., Leitzell, K., Lonnoy, E., Matthews, J. B. R., Maycock, T. K., Waterfield, T., Yelekçi, O., Yu, R., and Zhou, B., Book Section 6, Cambridge University Press, Cambridge, UK and New York, NY, USA, https://doi.org/10.1017/9781009157896.008, 2021.

Wang, H., Lu, X., Jacob, D. J., Cooper, O. R., Chang, K.-L., Li, K., Gao, M., Liu, Y., Sheng, B., Wu, K., Wu, T., Zhang, J., Sauvage, B., Nédélec, P., Blot, R., and Fan, S.: Global tropospheric ozone trends, attributions, and radiative

impacts in 1995–2017: an integrated analysis using aircraft (IAGOS) observations, ozonesonde, and multi-decadal chemical model simulations, Atmos. Chem. Phys., 22, 13753–13782, https://doi.org/10.5194/acp-22-13753-2022, 2022.

University of Washington: Mt. Bachelor Observatory, https://sites.uw.edu/jaffe-group/mt-bachelor-observatory/ (last access: 12 August 2023), 2023.

World Meteorological Organization: WMO Air Quality and Climate Bulletin – No. 2, September 2022, https://library.wmo.int/idurl/4/58736 (last access: 26 September 2023), edited by: Cooper, O. R., Carmichael, G., Laj, P., Nicely, J. M., Peuch, V.-H., Sokhi, R. S., Stein, A., and Walker, J., 2022.

Ziemke, J. R., Kramarova, N. A., Frith, S. M., Huang, L.-K., Haffner, D. P., Wargan, K., Lamsal, L. N., Labow, G. J., McPeters, R. D., and Bhartia, P. K.: NASA satellite measurements show global-scale reductions in free tropospheric ozone in 2020 and again in 2021 during COVID-19, Geophys. Res. Lett., 49, e2022GL098712, https://doi.org/10.1029/2022GL098712, 2022.